Photonic crystal-liquid crystal fibers for single-polarization or high-birefringence guidance

D. C. Zografopoulos, E. E. Kriezis, and T. D. Tsiboukis

Applied and Computational Electromagnetics Laboratory, Department of Electrical and Computer Engineering, Aristotle University of Thessaloniki, Thessaloniki GR-54124, Greece.

dzogra@auth.gr, mkriezis@auth.gr, tsibukis@auth.gr

Abstract: The dispersive characteristics of a photonic crystal fiber enhanced with a liquid crystal core are studied using a planewave expansion method. Numerical results demonstrate that by appropriate design such fibers can function in a single-mode/single-polarization operation, exhibit high- or low- birefringence behavior, or switch between an on-state and an off-state (no guided modes supported). All of the above can be controlled by the application of an external electric field, the specific liquid crystal anchoring conditions and the fiber structural parameters.

OCIS codes: (060.2400) Fiber properties; (230.3720) Liquid-crystal devices; (060.2420) Fibers, polarization-maintaining; (060.2430) Fibers, single-mode; (999.999) Photonic crystal fibers.

References and links

1. M. D. Nielsen, C. Jacobsen, N.A. Mortensen, J.R. Folkenberg, and H.R. Simonsen, "Low-loss photonic crystal fibers for transmission systems and their dispersion properties," Opt. Express **12,** 1372–1376 (2004), http://www.opticsexpress.org/abstract.cfm?URI=OPEX-12-7-1372.
2. T. Ritari, J. Tuominen, H. Ludvigsen, J.C. Petersen, T. Sørensen, T.P. Hansen, and H.R. Simonsen, "Gas sensing using air-guiding photonic bandgap fibers," Opt. Express **12,** 4080–4087 (2004), http://www.opticsexpress.org/abstract.cfm?URI=OPEX-12-17-4080.
3. S. Lorenz, Ch. Silberhorn, N. Korolkova, R.S. Windeler, and G. Leuchs, "Squeezed light from microstructured fibers: towards free-space quantum cryptography," Appl. Phys. B **73,** 855–859 (2001).
4. J. Broeng, D. Mogilevtsev, S. Barkou, and A. Bjarklev, "Photonic crystal fibers: a new class of optical waveguides," Opt. Fiber Techn. **5,** 305–330 (1999).
5. T.A. Birks, J.C. Knight, and P. St. Russell, "Endlessly single-mode photonic crystal fiber," Opt. Lett. **22,** 961–963 (1997).
6. T.-L. Wu and C.-H. Chao, "A novel ultraflattened dispersion photonic crystal fiber," IEEE Phot. Tech. Let. **17,** 67–69 (2005).
7. B. Zsigri, J. Lægsgaard, and A. Bjarklev, "A novel photonic crystal fibre design for dispersion compensation," J. Opt. A **6,** 717–720 (2004).
8. L.P. Shen, W.-P. Huang, G.X. Chen, and S.S. Jian, "Design and optimization of photonic crystal fibers for broad-band dispersion compensation," IEEE Phot. Tech. Let. **15,** 540–543 (2003).
9. K. Saitoh, M. Koshiba, T. Hasegawa, and E. Sasaoka, "Chromatic dispersion control in photonic crystal fibers: application to ultra-flattened dispersion," Opt. Express **11,** 843–852 (2003), http://www.opticsexpress.org/abstract.cfm?URI=OPEX-11-8-843.
10. A. Ferrando, E. Silvestre, and P. Andrés, "Designing the properties of dispersion-flattened photonic crystal fibers," Opt. Express **9,** 687–697 (2001), http://www.opticsexpress.org/abstract.cfm?URI=OPEX-9-13-687.
11. K.P. Hansen, "Dispersion flattened hybrid-core nonlinear photonic crystal fiber," Opt. Express **11,** 1503–1509 (2003), http://www.opticsexpress.org/abstract.cfm?URI=OPEX-11-13-1503.
12. G.P. Crawford, D.W. Allender, and J.W. Doane, "Surface elastic and molecular-anchoring properties of nematic liquid crystals confined to cylindrical cavities," Phys. Rev. A **45,** 8693–8710 (1992).

#9848 - $15.00 USD Received 2 December 2005; revised 8 January 2006; accepted 16 January 2006

13. S.V. Burylov, "Equilibrium configuration of a nematic liquid crystal confined to a cylindrical cavity," JETP **85,** 873–886 (1997).
14. F. Du, Y.-Q. Lu, and S.-T. Wu, "Electrically tunable liquid-crystal photonic crystal fiber," Appl. Phys. Lett. **85,** 2181–2183 (2004).
15. T.T. Larsen, A. Bjarklev, D.S. Hermann, and J. Broeng, "Optical devices based on liquid crystal photonic bandgap fibers," Opt. Express **11,** 2589–2596 (2003), http://www.opticsexpress.org/abstract.cfm?URI=OPEX-11-20-2589.
16. E.P. Kosmidou, E.E. Kriezis, and T.D. Tsiboukis, "Analysis of tunable photonic crystal devices comprising liquid crystal materials as defects," IEEE J. Quantum Electron. **41,** 657–665 (2005).
17. T.T. Alkeskjold, J. Lægsgaard, A. Bjarklev, D.S. Hermann, J. Broeng, J. Li, and S.-T. Wu, "All-optical modulation in dye-doped nematic liquid crystal photonic bandgap fibers," Opt. Express **12,** 5857–5871 (2004), http://www.opticsexpress.org/abstract.cfm?URI=OPEX-12-24-5857.
18. B. Maune, M. Lončar, J. Witzens, M. Hochberg, T. Baehr-Jones, D. Psaltis, A. Scherer, and Y. Qiu, "Liquid-crystal electric tuning of a photonic crystal laser," Appl. Phys. Lett. **85,** 360–362 (2004).
19. S.G. Johnson and J.D. Joannopoulos, "Block-iterative frequency-domain methods for Maxwell's equations in a planewave basis," Opt. Express **8,** 173–190 (2001), http://www.opticsexpress.org/abstract.cfm?URI=OPEX-8-3-173.
20. S.G. Johnson and J.D. Joannopoulos, "The MIT Photonic-Bands Package," http://ab-initio.mit.edu/mpb/.
21. B. Bahadur, *Liquid crystals: applications and uses*, vol. 1 (World Scientific Publishing, 1990).
22. X. Feng, A.K. Mairaj, D.W. Hewak, and T.M. Monro, "Nonsilica glasses for holey fibers," IEEE J. Lightwave Tech. **23,** 2046–2054 (2005).
23. M.J. Weber, *Handbook of optical materials* (CRC Press, 2003).
24. X. Feng, T.M. Monro, P. Petropoulos, V. Finazzi, and D. Hewak, "Solid microstructured optical fiber," Opt. Express **11,** 2225–2230 (2003), http://www.opticsexpress.org/abstract.cfm?URI=OPEX-11-18-2225.
25. K. Morishita and S. Yutani, "Wavelength-insensitive couplers made of annealed dispersive fibers," IEEE J. Lightwave Tech. **17,** 2356–2360 (1999).
26. Y. Jeong, B. Yang, B. Lee, H.S. Seo, S. Choi, and K. Oh, "Electrically controllable long-period liquid crystal fiber gratings," IEEE Phot. Tech. Let. **12,** 519–521 (2000).
27. A. Ferrando and J.J. Miret, "Single-polarization single-mode intraband guidance in supersquare photonic crystal fibers," Appl. Phys. Lett. **78,** 3184–3186 (2001).
28. K. Suzuki, H. Kubota, S. Kawanishi, M. Tanaka, and M. Fujita, "Optical properties of a low-loss polarization-maintaining photonic crystal fiber," Opt. Express **9,** 676–680 (2001), http://www.opticsexpress.org/abstract.cfm?URI=OPEX-9-13-676.
29. K. Saitoh and M. Koshiba, "Single-polarization single-mode photonic crystal fibers," IEEE Phot. Tech. Let. **15,** 1384–1386 (2003).
30. A. Argyros, N. Issa, I. Bassett, and M.A. van Eijkelenborg, "Microstructured optical fiber for single-polarization air guidance," Opt. Lett. **29,** 20–22 (2004).
31. S. Gauza, J. Li, S.-T. Wu, A. Spadło, R. Dąbrowski, Y.-N. Tzeng, and K.-L. Cheng, "High birefringence and high resistivity isothiocyanate-based nematic liquid crystal mixtures," Liq. Cryst. **32,** 1077–1085 (2005).
32. J. Li, S.-T. Wu, S. Brugioni, R. Meucci, and S. Faetti, "Infrared refractive indices of liquid crystals," J. Appl. Phys. **97,** Art. 073501 (2005).
33. C. Hu and J.R. Whinnery, "Losses of a nematic liquid-crystal optical waveguide," J. Opt. Soc. Am. **64,** 1424–1432 (1974).
34. M. Green and S.J. Madden, "Low loss nematic liquid crystal cored fiber waveguides," Appl. Opt. **28,** 5202–5203 (1989).
35. O. Frazão, J.P. Carvalho, and H.M. Salgado, "Low-loss splice in a microstructured fibre using a conventional fusion splicer," Microw. Opt. Tech. Let. **46,** 172–174 (2005).
36. J. H. Chong and M.K. Rao, "Development of a system for laser splicing photonic crystal fiber," Opt. Express **11,** 1365–1370 (2003), http://www.opticsexpress.org/abstract.cfm?URI=OPEX-11-12-1365.
37. S.G. Leon-Saval, T.A. Birks, N.Y. Joly, A.K. George, W.J. Wadsworth, G. Karakantzas, and P.St.J. Russell, "Splice-free interfacing of photonic crystal fibers," Opt. Lett. **30,** 1629–1631 (2005).

1. Introduction

Photonic crystal fibers (PCFs), or holey fibers, have been under intense study during the last years since they offer a promising alternative to conventional fibers for a wide range of applications, such as in telecommunication, sensor, or quantum cryptography technology [1-3]. Holey fibers are normally composed of a transverse periodical arrangement of air holes opened in some dielectric material - silica being the rule - which is broken by a defect core. Light can be guided through the fiber by two distinct mechanisms, namely the total internal reflection

#9848 - $15.00 USD Received 2 December 2005; revised 8 January 2006; accepted 16 January 2006

(TIR) and the bandgap effect [4]. Fiber guiding by the TIR effect relies on index-guiding by a core, whose refractive index is higher than the cladding's effective index, while the bandgap effect guiding holey fibers take advantage of the full 2-D bandgaps exhibited by the cladding's periodical structure, which confine light in a hollow core along the fiber axis.

Holey fibers operating under the TIR principle show some significant advantages compared to their conventional counterparts. For instance, they can be exclusively fabricated out of a single dielectric, thus avoiding interfaces between different materials that might undermine the fiber's performance. The dependence of the cladding's effective index on wavelength permits the manifestation of only a finite number of modes at relatively high frequencies, due to the reduction of the difference between the refractive indices of the core and the cladding for increasing frequencies [5]. Furthermore, it has been theoretically shown and experimentally verified that holey fibers with a triangular lattice of air-holes can exhibit endlessly single-mode operation provided the diameter of the cladding's air holes and the centre-to-centre spacing of two adjacent holes (lattice constant) are properly chosen [5].

The variation of the cladding's effective index can be optimally turned to advantage, as far as the fiber's dispersion properties are concerned. The wide tailoring of the fiber's design in terms of the air hole sizes, shapes and arrangements provides several degrees of freedom whose proper combination can tune the fiber's dispersion curve. The influence of the design parameters on the dispersion properties of holey fibers has been extensively studied, concerning both the classical triangular air hole-silica core lattice and other configurations that include additional features, e.g. air hole rings of variable diameter, air holes with elliptical cross-sections or doped-silica cylindrical cores [6-9]. Several types of holey fibers were designed that exhibit favorable dispersion properties, such as zero-dispersion at the 1.55 μm operation wavelength, and ultra-flattened group-velocity dispersion curves of zero, positive or negative dispersion over a significant wavelength regime [10-11].

Nematic liquid crystals are anisotropic materials consisting of rod-like molecules whose axis coincides with the anisotropy's optical axis. When confined in closed cylindrical cavities in the absence of external stimuli, the liquid crystal's director distribution is determined by the physics of elastic theory and the anchoring conditions at the cavity's surface [12-13]. Under the application of a static electric field the director's orientation can be controlled, since the liquid crystal molecules tend to align their axis according to the applied field. In an alternative approach, the properties of nematic liquid crystals can be tuned thermally owing to the dependence of the refractive index values on temperature. The above features have favored their utilization in a number of recently proposed photonic crystal based optoelectronic devices [14-18].

In this paper, we propose and theoretically analyze a novel photonic crystal - liquid crystal (PC-LC) core fiber design. Calculations are performed by solving for the eigenmodes of Maxwell's equations in periodic structures by a preconditioned conjugate-gradient minimization of the block Reyleigh quotient in a planewave basis [19], using an available software package [20]. The fiber consists of a triangular lattice of air holes opened in an optical glass enhanced by a hollow cylindrical core filled by common nematic liquid crystal, thus embodying both the design tailoring advantages of common holey fibers and the intrinsic controllable anisotropy of the liquid crystal material. The fiber's characteristics, namely modal dispersion curves, birefringence and modal intensity profiles are studied for a uniform distribution of the nematic director. Though this particular director orientation is in a sense ideal, it can be thought as the limiting orientation of more realistic patterns, and, in addition, it demonstrates the salient points for this special class of fibers. It is verified that the fiber can function in a single-mode/single-polarization operation (selectively HE_x or HE_y), it can exhibit high- or low-birefringence, or switch between on-off states, depending on the structural design.

#9848 - $15.00 USD Received 2 December 2005; revised 8 January 2006; accepted 16 January 2006

2. Photonic crystal-liquid crystal fiber analysis

2.1. Structural parameters and fiber layout

The fiber under study is shown in Fig. 1 and consists of three rings of a triangular lattice of air holes of radius r opened in a lossless optical fiber glass, whose refractive index n_g is considered constant. The transverse periodicity is broken by a defect core with diameter d_c. The core is filled with a typical nematic liquid crystal material characterized by ordinary and extraordinary refractive indices of n_o and n_e, respectively. The selection of the fiber materials is only limited by the requirement that the refractive index of the fiber glass matches the extraordinary index of the nematic liquid crystal, as will be evidenced by the analysis hereafter. Extraordinary indices within the range $1.5 < n_e < 1.8$ are typical for nematic materials [21], and their values can be sufficiently tuned by factors such as molecular design, chemical synthesis conditions, and operating temperature. Additionally, nonsilica fiber glasses whose refractive index obtains values as high as $n_g = 2.2$ are commercially available and they have already been proposed and studied as candidates for the fabrication of holey fibers [22]. Among the various types of available fiber glasses for which $1.5 < n_g < 1.8$ are the high-lead silicate, barium crown, lanthanum crown, or barium flint fiberglasses [23]. The refractive index of these glasses can be tuned, for instance, by adjusting the doping percentage of metal oxides such as lead (PbO) or lanthanum (La_2O_3) oxides. Particular examples of high index glasses in the above range were reported in [24-25]; in the first reference a lead oxide borosilicate glass of $n_g = 1.76$ was utilized in making microstructured optical fibers, whereas in the second a barium crown glass of $n_g = 1.61$ was adopted in a conventional wavelength insensitive coupler. For the purposes of the present analysis we selected the common nematic material E7 ($n_e = 1.68$, $n_o = 1.5$) and a fiberglass with $n_g = 1.68$. The fiber is considered to be uniform along the z-axis, which coincides with the axis of the cylindrical defect core.

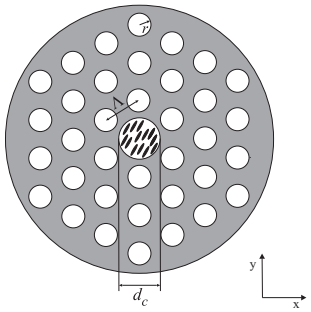

Fig. 1. Cross-sectional view of the proposed type of PC-LC fiber: hole-to-hole spacing Λ, hole radius r, and central defect core diameter d_c. The figure corresponds to parameters $r = 0.2\Lambda$, and $d_c = \Lambda$.

Before proceeding to the analysis of the LC-PC fiber, we provide a reference diagram (Fig. 2) where the dispersion curve for the fundamental degenerate HE_x and HE_y modes, along with the dispersion curve of the first higher order mode and the cladding's fundamental space-filling mode (FSM) - namely the radiation line - are plotted for a conventional (solid core) photonic crystal fiber with $n_g = 1.68$ and $r = 0.2\Lambda$. Noticeable in the figure, the fiber is endlessly-single mode; the first higher-order mode dispersion curve always remains below the radiation line (see inset in Fig. 2).

We study the case where the nematic director in the fiber core is uniform and parallel to the x- or y-axis of the fiber's lattice. Such alignment can be theoretically exhibited under the influence of the appropriate homeotropic anchoring conditions. The planar-polar (PP) profile, a

#9848 - $15.00 USD Received 2 December 2005; revised 8 January 2006; accepted 16 January 2006

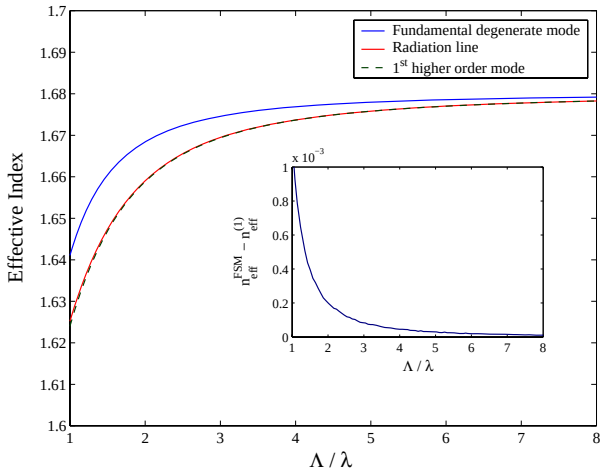

Fig. 2. Dispersion curve for the degenerate HE_x and HE_y modes of a triangular lattice PCF with $r = 0.2\Lambda$ and $n_g = 1.68$. The notations n_{eff}^{FSM} and $n_{eff}^{(1)}$ refer to the effective indices of the FSM mode and the first higher order mode, respectively.

commonly observed director pattern for nematic liquid crystals confined in cylindrical capillaries comprises an example, where almost uniform alignment of the director can be achieved. In general, the PP texture can be analytically calculated [12] under the one elastic constant approximation $K_{11} = K_{33} = K$ for the nematic material. The Euler-Lagrange equation for minimizing the elastic free energy takes the form of the two-dimensional Laplace equation (1), expressed in polar coordinates,

$$\frac{\partial^2 \psi(r,\phi)}{\partial r^2} + \frac{1}{r}\frac{\partial \psi(r,\phi)}{\partial r} + \frac{1}{r^2}\frac{\partial^2 \psi(r,\phi)}{\partial \phi^2} = 0, \tag{1}$$

ψ being the angle between the director and the radial unit vector. The solution of (1) yields the following relation

$$\psi(r,\phi) = \frac{\pi}{2} - \tan^{-1}\left[\frac{(R^2+\gamma r^2)}{(R^2-\gamma r^2)}\tan\phi\right], \tag{2}$$

where $\gamma = (\xi^2+1)^{1/2} - \xi$, $\xi = 2K/RW_0$ and RW_0/K is the effective anchoring strength, which determines the orientation of the molecules at the cavity wall. At the strong anchoring limit the director is locally perpendicular to the surface (Fig. 3(a)), while as the anchoring strength relaxes, the molecules tend to adopt a more uniform orientation towards the uniform profile acquired at the weak anchoring limit (Fig. 3(b)).

Another way to generate the uniform profile is by controlling the nematic director through the application of an external electric (or magnetic) static field. Figure 4 shows how the application of a sufficiently strong voltage [26] between two pairs of electrodes can align the nematic molecules along the x- or y-axis and lead to an almost uniform director profile.

2.2. Single-mode/single-polarization guidance

The uniform alignment of the nematic director has a direct impact on the fiber's waveguiding behaviour. Let us assume, for instance, the profile of Fig. 3(b), were the optical axis coincides with the y-axis. Owing to the birefringence of the defect core's nematic material, the effective refractive index of the core shall differ for light of different polarizations. In the case of

#9848 - $15.00 USD Received 2 December 2005; revised 8 January 2006; accepted 16 January 2006

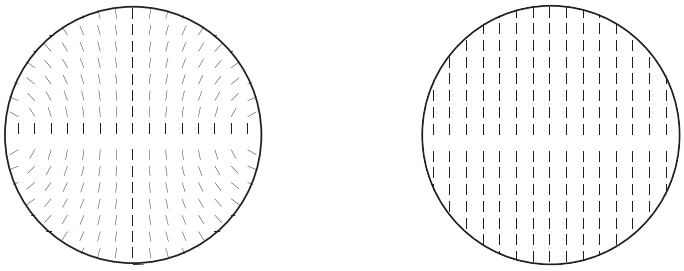

Fig. 3. The planar-polar director profile at the strong (a) and the weak (b) anchoring limit.

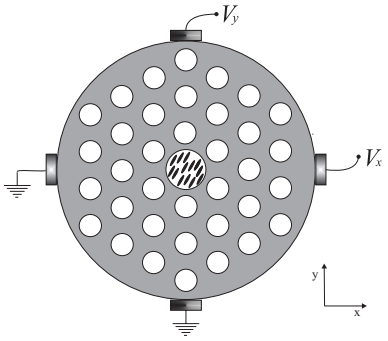

Fig. 4. Layout for arbitrarily controlling the orientation of the nematic director profile in the xOy plane: for instance, uniform x-parallel alignment ($V_x = V_0$, $V_y = 0$), and uniform y-parallel alignment ($V_y = V_0$, $V_x = 0$).

y-polarized light, the core is practically homogenous - since we have assumed that for the fiberglass and the chosen nematic material the condition $n_g = n_e$ is met - and, therefore, the fiber's operation in this case shall not differ significantly from a common solid core PCF. Thus, the fiber can exhibit properties such as the endlessly-single mode operation provided that the cladding's hole radius is smaller than a threshold value. On the contrary, a x-polarized field senses a more complex core region where a low-refractive index cylinder is embedded in the fiberglass background. A rough estimation of the core's effective refractive index $n_{eff,x}^{core}$ at the low-frequency regime is obtained by considering the core as a region occupied by two circular discs with radii r_{def} and $r_{core} = 0.5\Lambda$ [5]; the effective index $n_{eff,x}^{core}$ referring to the x- polarization, is then given by

$$n_{eff,x}^{core} = n_e \left[1 - \left(\frac{2r_{def}}{\Lambda} \right)^2 \right] + n_o \left(\frac{2r_{def}}{\Lambda} \right)^2, \quad \lambda >> \Lambda. \tag{3}$$

The total internal reflection waveguidance criterion at a given wavelength λ demands that the core's effective index is higher than that of the cladding. In the case studied, this criterion is interpreted as $n_{eff}^{clad}(\lambda) < n_{eff,x}^{core}(\lambda)$, where $n_{eff}^{clad}(\lambda) \equiv n_{eff}^{FSM}(\lambda)$ is the index of the cladding's fundamental space-filling mode. Thus, the satisfaction of the opposite condition ($n_{eff}^{clad}(\lambda) > n_{eff,x}^{core}(\lambda)$) within a wavelength range of interest is expected to permit the exhibition of single-polarization (HE_y) operation. Single-polarization PCFs have also been proposed based on a special design of the cladding [27-30], lacking, though, the versatility of selective operation between the two polarizations (HE_x either HE_y) of the proposed fiber.

#9848 - $15.00 USD Received 2 December 2005; revised 8 January 2006; accepted 16 January 2006

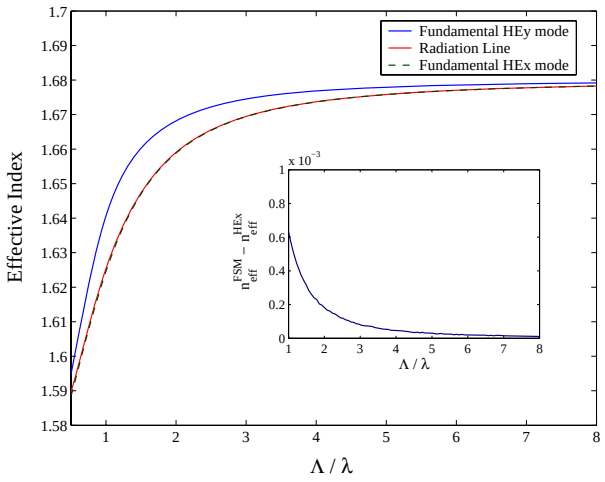

Fig. 5. Dispersion curves for the fundamental HE_x and HE_y modes and radiation line for the PC-LC fiber of Fig. 4 in the planar polar weak anchoring limit case for $r_{def} = 0.5\Lambda$ and $r = 0.2\Lambda$. As noticed, the fiber exhibits both endlessly single-mode and single-polarization behavior.

Furthermore, in case the fiber is also endlessly-single mode, the HE_y shall be the only mode allowed to propagate. This is not hard to achieve; for the fiber proposed, let $r = 0.2\Lambda$, $r_{def} = 0.5\Lambda$, and, therefore, $n_{eff,x}^{core} \simeq n_o = 1.5$, which is lower than $n_{eff}^{clad}(\lambda)$ at all wavelengths (see radiation line of Fig. 2). Figure 5 shows the modal dispersion curves of the PC-LC fiber for $r_{def} = 0.5\Lambda$. The HE_y modal dispersion curve is similar to that of the degenerate HE_x and HE_y modes of the reference solid core PCF of Fig. 2. Moreover, the HE_y mode's intensity profile at $\Lambda/\lambda = 1.5$ (Fig. 6(a)) is identical to the fundamental mode's profile of a common PCF. On the other hand, the dispersion curve of the fundamental HE_x remains below the radiation line (Fig. 5) and its intensity profile at $\Lambda/\lambda = 1.5$ (Fig. 6(b)) clearly shows that it corresponds to an evanescent mode.

2.3. Controllable birefringence guidance

The next step is to investigate the influence of the core's radius on the fiber's dispersive characteristics. The reduction of the defect radius is expected to lead to the emergence of the fundamental HE_x modal curve above the radiation line, into the waveguiding region due to the gradual increase of $n_{eff,x}^{core}$. As the defect radius tends towards the limit $r_{def} \to 0$ the HE_x dispersion is expected to rise towards the curve of the HE_y mode, which is independent of the defect radius. Thus, the continuous decrease of r_{def} below a critical value r_{def}^{cr} shall controllably tune the HE_x curve. No other guided modes are expected to appear since the fiber's endlessly single-mode condition continues to be valid. As a conclusion, the fiber may pass from a single-mode single-polarization operation to a single-mode operation of controllable birefringence. The birefringence for the fundamental mode theoretically becomes zero for $r_{def} \to 0$ and is expected to obtain a maximum value around $r_{def} \simeq r_{def}^{cr}$, marginally equal to the difference between the HE_y curve and the radiation line.

Additional simulations proved the reasoning of the above insights. Figure 7 shows the dispersion curves of the HE_x mode for various values of r_{def}, along with the invariable HE_y curve and the radiation line. The value r_{def}^{cr} below which the HE_x mode starts to propagate was found approximately $r_{def}^{cr} = 0.25\Lambda$. For lower values of r_{def} the HE_x curves move towards the upper

#9848 - $15.00 USD Received 2 December 2005; revised 8 January 2006; accepted 16 January 2006

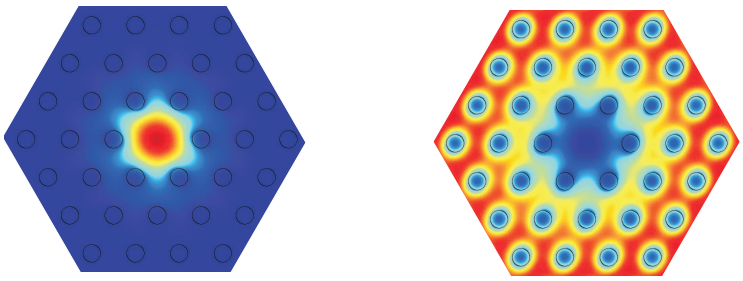

(a) (b)

Fig. 6. Modal intensity profiles at $\Lambda/\lambda = 1.5$ for the fundamental y- and x-polarized modes for the dispersion curves of Fig. 5: a) HE_y mode for $r_{def} = 0.5\Lambda$, b) HE_x mode for $r_{def} = 0.5\Lambda$. The air hole radius is $r = 0.2\Lambda$. The HE_y mode, which senses a homogenous core of $n_e = 1.68$, shows a regular hexagonal profile. On the contrary, the HE_x mode radiates into the cladding.

limit of the HE_y curve. The HE_x modal intensity profile at $\Lambda/\lambda = 1.5$ for various core radii are shown in Fig. 8. Moreover, there is another observation of significant interest. The HE_x dispersion curves for $r_{def} = 0.2\Lambda$ and $r_{def} = 0.25\Lambda$ do not continue until the high-frequency regime; instead, they disappear below the radiation line after a frequency threshold (see inset of Fig. 7). This threshold was found at $\Lambda/\lambda \simeq 2$ for $r_{def} = 0.25\Lambda$ and $\Lambda/\lambda \simeq 5$ for $r_{def} = 0.2\Lambda$. It seems that the part of the HE_x dispersion curves that enters the waveguidance region is, in general, a part of a modal curve which drops below the radiation line above a certain threshold frequency. This can be attributed to the weaker concentration of the electric field in the high index area of the core for high frequencies compared to that of the respective cladding modes, which confine light more severely in the dielectric, given that the dielectric contrast of the cladding is higher than that of the defect core. Thus, for high frequencies the radiation line approaches the limit of n_g staying above the HE_x dispersion curves of the x-polarized guided modes. This fact is taken into account in Fig. 9, where the modal birefringence curves for each case are truncated at the respective threshold frequency.

Figure 9 shows that especially high values of modal birefringence can be achieved, up to 1.4×10^{-2} for the $r_{def} = 0.25\Lambda$ curve. Theoretically the value of birefringence could be further raised by two distinct mechanisms, e.g. by raising the fundamental HE_y curve, or lowering the radiation line, so that the greater gap emerging could be optimally exploited. One way of achieving such a gap broadening is by selecting a nematic material with particularly high optical anisotropy and refractive index values. In our simulations we assumed the nematic E7, which has a birefringence between $\Delta n = 0.18$ and $\Delta n = 0.2$ at usual operating frequencies [32], yet mixtures of nematic liquid crystals whose birefringence obtains values as high as $\Delta n = 0.4$ ($n_o = 1.5$, $n_e = 1.9$) have also been reported [31]. The choice of such nematic materials, provided that an appropriate fiberglass is selected that meets the matching condition $n_g = n_e$ may, therefore, lead to higher values of birefringence. The depression of the radiation line can be easily achieved by enlarging the holes of the triangular lattice. Nevertheless, such a modification would instantly lift the endlessly-single mode condition leading to the appearance of extra modes in the guidance regime. We examined the influence of the magnification of the lattice

#9848 - $15.00 USD Received 2 December 2005; revised 8 January 2006; accepted 16 January 2006

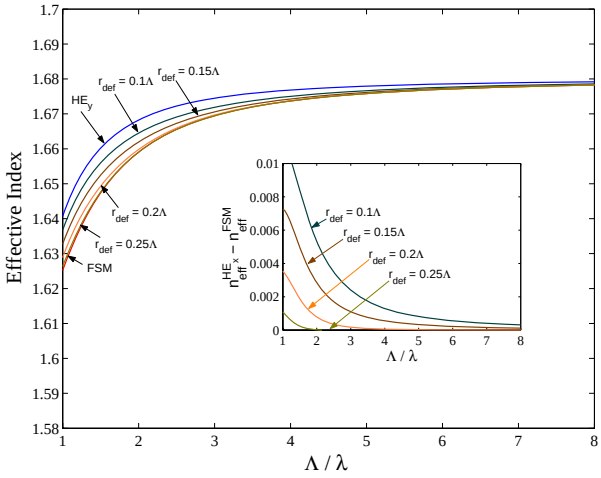

Fig. 7. Dispersion curves for the fundamental HE_x and HE_y modes and radiation line for the planar polar weak anchoring limit case. HE_x mode curves correspond to different r_{def} values.

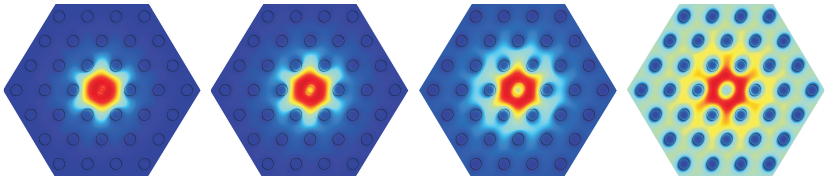

Fig. 8. Modal intensity profiles at $\Lambda/\lambda = 1.5$ for the fundamental x-polarized mode for different radii of the defect core: a) $r_{def} = 0.1\Lambda$, b) $r_{def} = 0.15\Lambda$, c) $r_{def} = 0.2\Lambda$, and d) $r_{def} = 0.25\Lambda$. The radius of the air holes is kept constant at $r = 0.2\Lambda$.

holes in the case of $r_{def} = 0.3\Lambda$, where the fiber exhibits the single-mode/single-polarization property for $r = 0.2\Lambda$. For a hole-radius of $r = 0.25\Lambda$ the fiber was found to be multimode for $\Lambda/\lambda > 2$, while for $r = 0.3\Lambda$ the threshold between single-mode and multi-mode operation was found at $\Lambda/\lambda \simeq 1.5$. The modal birefringence, though, obtains its maximum value in the single-mode regime, found equal to 2.99×10^{-2} at $\Lambda/\lambda = 1$ and 4.11×10^{-2} at $\Lambda/\lambda = 0.95$ for $r = 0.25\Lambda$ and $r = 0.3\Lambda$, respectively. Depending on the application, the limitation of the single-mode frequency regime might be of lesser significance than the achievement of such high birefringence values.

Another point of interest is the investigation of the fiber's properties when the condition $n_g = n_e$ is relaxed. As the equality refers to an ideal case, it is possible that this condition cannot be met exactly in practice, at least for broad wavelength ranges, such as those of the present analysis. We will assume that the refractive indices of the nematic material are kept fixed, while that of the glass can obtain values around n_e. In case $n_g < n_e$, the core obtains a more intense guiding behavior, while the radiation line, which depends solely on the fiberglass cladding, is expected to drop; these modifications shall eventually lead to the emergence of more propagating modes, turning the fiber from single-mode to multimode. On the contrary, if $n_g > n_e$ the radiation line rises and, thus, no more propagating modes emerge. In addition, the fundamental

#9848 - $15.00 USD Received 2 December 2005; revised 8 January 2006; accepted 16 January 2006

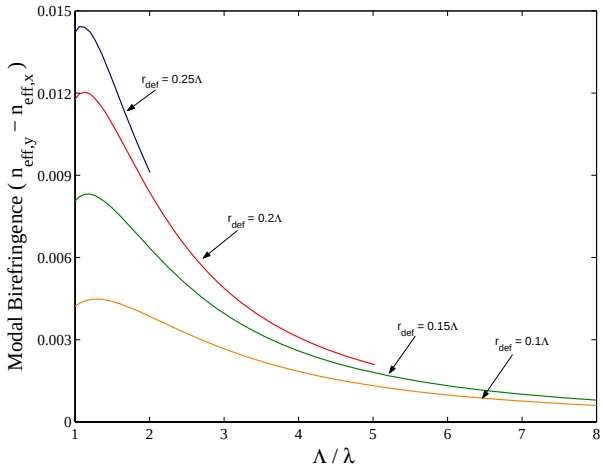

Fig. 9. Modal birefringence of the fundamental HE_x and HE_y modes for $r_{def} = 0.1\Lambda$, 0.15Λ, 0.2Λ, and 0.25Λ.

single-polarized mode's dispersion curve is bound to drop below the radiation line at a certain frequency threshold, above which the fiber shall support no guided modes whatsoever. Figure 10 elucidates the reasoning of the above remarks; for $n_g = 1.67$ the fiber supports a second guided mode for $\Lambda/\lambda > 3$ (Fig. 10(a)), while for $n_g = 1.69$ the fiber ceases to guide any modes for $\Lambda/\lambda > 4$. In both cases, though, the fiber is shown to operate under the single-mode single-polarization property within a large wavelength regime, despite the deviation from the ideal condition $n_g = n_e$.

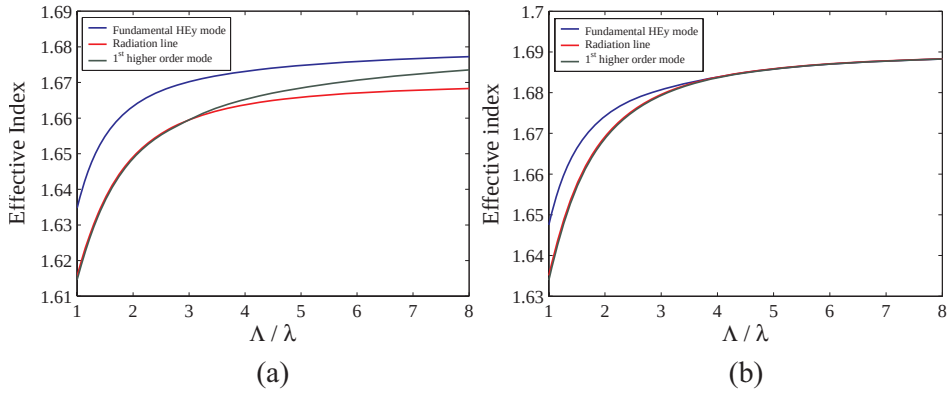

Fig. 10. Modal dispersion curves for (a) $n_g = 1.67$ and (b) $n_g = 1.69$. The parameters used in both cases are $r = 0.2\Lambda$, $r_{def} = 0.4\Lambda$, $n_o = 1.5$, and $n_e = 1.68$.

2.4. Switching between on-off states

Finally, we shall examine the case of a uniform director profile where the optical axis is now parallel to the z-axis (axial configuration). This profile can be exhibited under homogenous anchoring conditions and can be at large approached under homeotropic anchoring condition at the weak anchoring limit of the escaped - radial (ER) configuration. The director for the

#9848 - $15.00 USD Received 2 December 2005; revised 8 January 2006; accepted 16 January 2006

ER pattern remains radial on the transverse plane very close to the cavity wall, yet escapes in the third dimension while moving towards the cylinder axis. The director profile in polar coordinates is given by

$$\psi(r,\phi) = 0, \tag{4}$$

$$\theta(r) = \frac{\pi}{2} - 2\tan^{-1}\left(\frac{r}{R}\tan(a/2)\right), \tag{5}$$

where ψ, θ are the angles between the director and the radial unit vector and the z-axis, respectively, $a = \pi/2 - \theta(r = R) = \cos^{-1}(1/\sigma)$, and $\sigma = RW_0/K + K_{24}/K - 1$ is the parameter that expresses the anchoring strength, considered to be larger than unity. In the case of strong anchoring conditions ($\sigma \to \infty$) the molecules are perpendicularly aligned to the cavity wall (Fig. 11(a)). While moving towards the weak anchoring limit ($\sigma = 1$) the molecules obtain an alignment parallel to the z-axis (Fig. 11(b)).

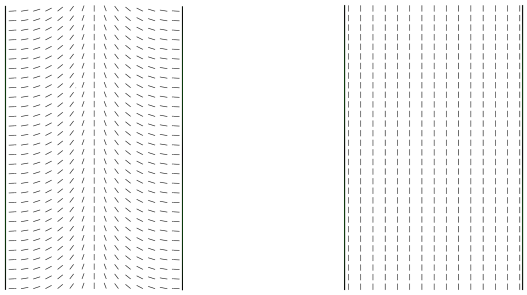

Fig. 11. The escaped - radial profile at the strong (a) and the weak (b) anchoring limit.

For the axial profile of Fig. 11(b) it is implied that both polarizations on the transverse plane shall sense an effective core index of $n_o = 1.5$, which prevents the emergence of any propagating modes whatsoever. Figure 12 shows the modal dispersion plot for the axial director profile case; it is verified that all modes remain below the radiation line, and therefore the fiber, in practice, operates in an off-mode state. Actually, the LC molecules need not be strictly parallel to the fiber axis. The escaped-radial pattern of Fig. 10(a) can also allow for an off-mode operation since the effective index of the core need not be necessarily as low as 1.5. In the analysis so far, we have observed that even down to the threshold value of $r_{def} \simeq 0.25\Lambda$ the polarization that senses a core of n_o is not allowed to propagate. This implies that the ER profile in a larger core is expected to lead to an effective core index low enough to inhibit the presence of any guided modes whatsoever, given the degeneracy of the HE_x and HE_y due to the ER profile's symmetry.

Thus, a fiber exhibiting the above texture (ER) under the application of an external electric field - with electrodes placed as in Fig. 4 - can operate alternatively in a single-polarization single-mode operation for $V_{x,y} \geq V_{th}$ (director parallel to the x- or y- axis) and an off-mode state for $V_{x,y} = 0$ (director parallel to the z-axis). This property could be exploited for instance in switching protection applications of optical streams, with the switching speed solely limited by the response time of the LC molecules. Response times in the order of a few ms are typical for nematic liquid crystals, providing a switching performance compliant with telecommunication standards, such as those of the Synchronous Digital Hierarchy (SDH), which require a protection switchover in less than 50 ms.

A final issue regarding the potential use of such fibers in optical systems is that of the involved overall losses. The principal loss mechanisms in this case are absorption and scattering losses associated with the nematic material. It has been shown that bulk scattering losses obtain

#9848 - $15.00 USD Received 2 December 2005; revised 8 January 2006; accepted 16 January 2006

values two orders of magnitude higher than absorption, ranging between 15∼40 dB/cm [33]. Fortunately, scattering loss is significantly suppressed (1∼3 dB/cm) in case the nematic material is confined in capillaries of small core diameter (2∼8 μm) [34]. Leakage losses due to the finite dimensions of the fiber can be minimized by adding more ring holes in the periodic cladding. Finally, numerous studies have shown that splicing issues between conventional and microstructured fibers can also be addressed; splicing losses of 0.2∼0.9 dB have been reported for various techniques such as arc-fusion splicing [35] or laser splicing [36], and a method for the formation of a splice-free low-loss interface between the two fiber types has been also successfully implemented [37].

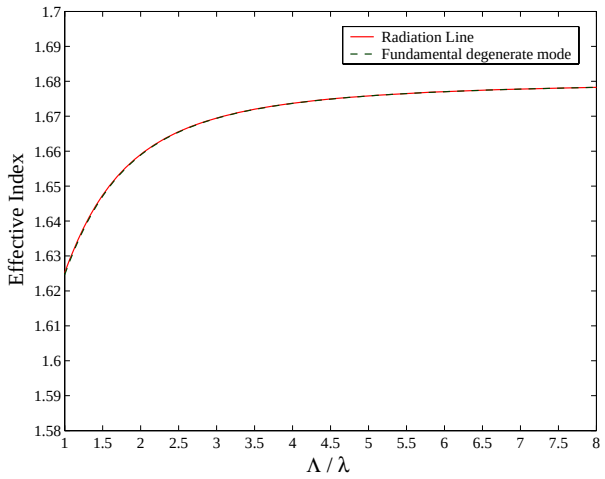

Fig. 12. Dispersion curves for the axial director profile case for $r_{def} = 0.5\Lambda$ and $r = 0.2\Lambda$. The fiber operates in an off-state since all supported modes are evanescent.

3. Conclusions

A novel liquid-crystal core photonic-crystal fiber design has been proposed for single-polarization and high-birefringence fibers. It was found that the proposed type of nematic core fibers can support an endlessly single-mode/single-polarization operation under the appropriate anchoring conditions. It is noteworthy that the fiber's lattice symmetry is not disturbed; thus, no orientation issues arise concerning the coupling and splicing problems that appear for single-polarization fibers with stress induced or geometrical birefringence. Moreover, under the control of an external electric field, the fiber proved capable of functioning with preferential polarization characteristics, a feature that might be directly exploited in polarization control elements or other similar devices. In addition, the fiber design allows for the fabrication of fibers with controllable birefringence values, from remarkably high values (more than 4×10^{-2}) down to zero birefringence. More realistic patterns of the nematic director as well as other nematic materials are currently under investigation, in order to predict the fiber's behaviour under different conditions; these will be reported in the context of a future publication.

#9848 - $15.00 USD Received 2 December 2005; revised 8 January 2006; accepted 16 January 2006